International Journal of Infrared and Millimeter Waves, Vol. 14, No. 10, 1993

QUASI-OPTICAL MEASUREMENT OF COMPLEX DIELECTRIC CONSTANT AT 300 GHz

Bernd Stöckel

Lehrstuhl für Hochfrequenztechnik
Universität Erlangen-Nürnberg
Cauerstr. 9, D-91058 Erlangen
Germany

Received July 17, 1993

1 Abstract

A two beam interferometer in the Martin-Puplett configuration is used to determine the complex dielectric constant at 300 GHz of teflon, TPX-plastics, SPECTRALON and paraffin waxes with melting temperatures of 48° C and 72° C, respectively. The design of the quasi-optical system leads to a constant beam diameter at the power detector independent of path delay and frequency. The power detector signal is recorded not only along one period but over about 50 periods. A spectrum estimation routine allows to determine more exactly amplitude and phase angle of the signal. A basic problem is noticed: imperfect detector and source match cause harmonic distortion of the power detector signal. The effects on processing the loss tangent and the invalidation are shown. Finally loss tangent and dielectric constant are determined indirectly by optimizing an equivalent microwave circuit using a commercial available microwave design system to take multiple reflections and losses in consideration.

Keywords: Quasi-optics, interferometer, dielectric constant, loss tangent, TPX, teflon, SPECTRALON, paraffin, harmonic distortion, complex overlap integral

2 Introduction

Much work and effort have been taken in the field of measuring the optical properties of materials in the (sub)mm-wave region (30 GHz - 3 THz). The paper of Simonis [1] for example, who collected 170 citations dealing with measurements of optical properties in the frequency range up to 1000 GHz, gives an idea of that. The amount of publications represents a basic problem for every (sub)mm-group. On the one hand commercial suppliers can often not provide information about optical properties of the offered materials in the (sub)mm-wave region. On the other hand there are often problems in manufacturing materials with reproducible constant optical properties. So in general it is a necessity to measure the dielectric materials which you want to use for lenses, windows, beam-splitters, dielectric lines, antireflecting coatings, multi-layer interference filters, etc. by yourself and at that frequency you want to work at. An overview of all commonly used techniques is given by Afsar [2]. But which kind of technique should be utilized? It seems, that in general the method of single-frequency dual-beam interferometry should be preferred to resonator-techniques and Fourier-transform-spectroscopy because of simplicity of equipment: the method of dual-beam interferometry only needs basic equipment of a (sub)mm-group as a source (often a laser), beam guiding elements, beam splitters and combiners and a power detector. Other methods require high power broadband noise sources, high sensitive broadband power detectors, resonators with high quality factor and frequency tuneable sources, which are often not available.

The principle of measuring optical properties with a dual-beam interferometer is well known ([3],[4],[5]). Nevertheless many steps and traps have to be overcome.

- In this paper another method is proposed to get a more precise value of the phase angle information: a spectrum estimation routine in connection with a special coupling of the Gaussian beams to the power detector due to a special quasi-optical beam-guiding system.

- Another method is proposed to get the desired complex dielectric constant from amplitude and phase angle information. An equivalent microwave circuit of the sample is simulated (for plane waves) in TOUCHSTONE[1] (so multiple reflections and ohmic losses are

[1]TOUCHSTONE is a product of EESof

taken in consideration), and loss tangent and dielectric constant are changed by an optimizing routine so that measured data correspond to simulated data. In contrast to other papers here phase angle and amplitude information are obtained by one measurement.

- In the course of experiments it is observed that the power detector signal is harmonically distorted. This can be explained by imperfect source/load match. Its effects (mainly to loss tangent) and its improvement are shown. This may be the reason for great differences in loss tangent data of published measurements.

- It is shown that amplitude and phase angle deviations due to imperfect interfering of delayed and undelayed beam can be neglected. For that purpose the complex overlap integral of delayed and undelayed beam is evaluated across the sensitive area of the power detector.

- And last but not least experimental results are presented. Besides data of TPX[2]-plastics and teflon, also data of SPECTRALON[3] and paraffin waxes are presented, which can rarely be found in literature.

3 Measurement System

The measurement system (fig. 1) consists of a source, an interferometer with beam-guiding system, a power detector and a computer for controlling. The carcinotron source produces an output power up to 20 mW in the frequency range between 280 and 300 GHz. An interferometer in the Martin-Puplett configuration [6] is utilized. In the (sub)mm-wave region the Martin-Puplett interferometer is preferred to a Mach-Zehnder interferometer because of compact construction, simple realization of 50% beam splitters and combiners by polarization grids and simple realization of the phase shifter by a moveable rooftop mirror for the delay. It has to be taken into account that the sample, which can be inserted in the fixed arm of the interferometer, is passed twice by the beam. The signal of the power detector (a pyroelectric detector ELTEC 400) is amplified and fed to the computer. The interferometer is driven in the socalled fast scan-mode: The moveable mirror is shifted with a constant speed, so that no additional modulating is necessary for the pyroelectric

[2]TPX is delivered by Mitsui Petrochemical Industries LTD
[3]SPECTRALON is delivered by Labsphere

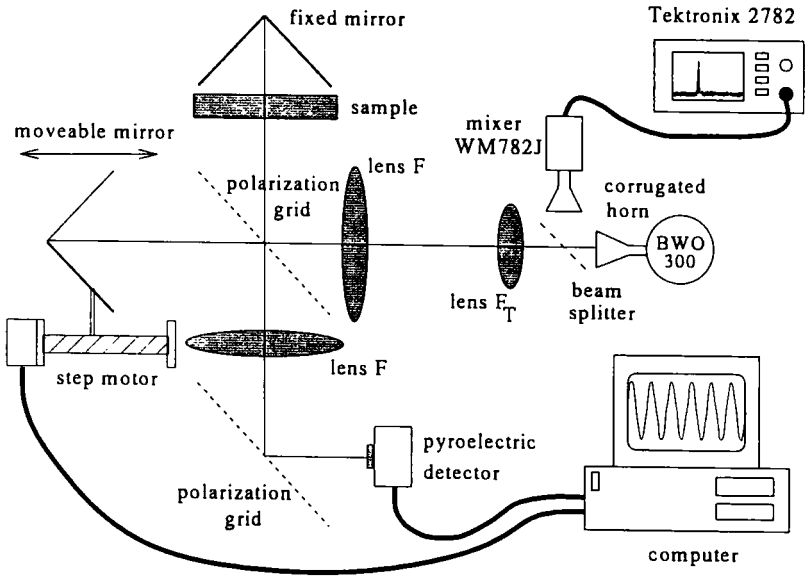

Figure 1: Schematic drawing of the measurement system

detector. The resulting modulation frequency is about 2 Hz, so that the pyroelectric detector operates in its most sensitive frequency range. Furthermore the time of measurement is reduced drastically, because less integration time is needed. The motion of the mirror is done by a step motor controlled by the computer. One step corresponds to a shift of 5 μm.

At first the power signal is recorded without the sample. The record serves as an amplitude and phase angle reference. Then the sample is inserted, and again the power signal is recorded with the same starting point of the mirror as before. So the system works as a quasi-optical homodyne vector network analyzer for transmission measurements ($U_{det} \sim \sqrt{P_{RF}}$). To monitor the frequency and the frequency shift of the free running carcinotron a spectrum analyzer (TEKTRONIX 2782 with harmonic mixer WM782J) is coupled to the source via a beam splitter. The frequency shift during a measurement of one sample is in the order of 1 - 2 MHz. This is achieved after a warm-up time of one hour.

4 Beam-Guiding System

In fig. 2 the unfolded beam-guiding system is scetched. It consists of a corrugated horn as beam source, a beam splitter to enable frequency controlling, a first lens for matching, two other lenses and at last the power detector. Because of clearness polarization grids and rooftop mirrors are omitted. The delicate problem is, how to guarantee a good coupling to the sensitive area of the power detector and interfering of the two beams (delayed and undelayed with optionally inserted sample)? The detecting area of the pyroelectric detector used is 2 mm in diameter. At a wavelength of about 1 mm in general it is not possible to concentrate the beam energy completely on it. Consequently spill-over losses occur in dependence upon the beam diameter at the power detector. The beam, which suffers different path lengths, will produce different beam diameters, so that the power detector signal strongly depends on the amount of delay.

Let us first start with the corrugated horn. It is flare-angle-limited, i.e. produces a Gaussian beam having a waist radius proportional to the wavelength [7]. The first matching lens fulfills two functions. For its location in the distance of its focal length from the horn antenna it changes the behavior of a flare-angle-limited into one of an aperture-limited horn antenna (far-field divergence angle proportional to the wavelength) and produces a much less divergent beam. Let us suppose the corrugated

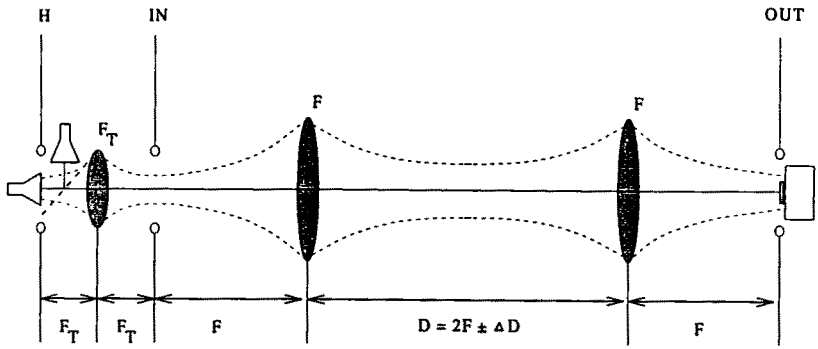

Figure 2: Schematic drawing of the unfolded beam-guiding system

horn produces a Gaussian beam with a waist radius w_{0H} being proportional to the wavelength λ_0 with $w_{0H} = p\lambda_0$. Then the transformed beam has the waist w_{0IN} at the distance F_T behind the lens with the focal length F_T:

$$w_{0IN} = \frac{F_T \lambda_0}{\pi w_{0H}} = \frac{F_T}{\pi p} = \text{const}(\lambda_0) \tag{1}$$

The following two lenses have equal focal lengths F and are separated by a certain distance D. The input waist w_{0IN} is located in the distance F in front of the first lens with the focal length F. And also the power detector is located in the distance F behind the second lens with the focal length F. The transformation matrix $\underset{\cdot}{T}$ of this system with input and output planes as shown in fig. 2 is given by [8]:

$$\underset{\cdot}{T} = \begin{pmatrix} -1 & 0 \\ \Delta D/F^2 & -1 \end{pmatrix} \qquad \text{with} \qquad \Delta D = D - 2F \tag{2}$$

Due to the nought in the transformation matrix $\underset{\cdot}{T}$ [8] the output beam has the beam radius w_{OUT} (this is not compelling the waist!) and the phase curvature radius r_{OUT} at the output plane of this system :

$$w_{OUT} = w_{0IN} \tag{3}$$

and

$$r_{OUT} = -\frac{F^2}{\Delta D} \tag{4}$$

Therefore the beam diameter at the power detector is independent of frequency and the distance between the two lenses, which includes the path delay! For the fixed beam $\Delta D = 0$ is chosen, so that the transformed beam has its waist at the power detector independent of frequency in size and position. So the power of the undelayed and delayed beam is detected constantly without being affected by amount of path delay or frequency in any way. In tab. 1 the relevant values of the beam-guiding system are shown.

F_T in mm	F in mm	ΔD in mm	w_{OUT} in mm
40	220	-100 ...+100	11

Tabular 1: Relevant values of the beam-guiding system

Up to this point delayed and undelayed beam are considered separately. But what is about the efficiency of interfering of them? The Gaussian beams may have beam radii w_1, w_2, phase curvature radii r_1, r_2 at the distances $z_{1/2}$ to the waist position and the beam waist radius w_0. Then with R as the distance from the axis of propagation (z-axis) and the amplitude K the transverse variations of their electrical fields $E_{1/2}$ are given by [7]:

$$E_{1/2} = \frac{K w_0}{w_{1/2}} \exp\left[-\frac{R^2}{w_{1/2}^2} - \frac{\pi R^2}{\lambda_0 r_{1/2}} + j \arctan\left(\frac{\lambda_0 z_{1/2}}{\pi w_0^2}\right)\right] \tag{5}$$

The complex overlap integral C describes the interference of the two beams over the cross-sectional area A_C:

$$C = \frac{\int_{A_C} E_1 E_2^* dA_C}{\sqrt{\int_{A_C} E_1 E_1^* dA_C}\sqrt{\int_{A_C} E_2 E_2^* dA_C}} \tag{6}$$

For an infinite cross-sectional area ($A_C = A_{inf}$) it is analytically given by [9]:

$$C_{inf} = 2\left[\frac{w_1}{w_2} + \frac{w_2}{w_1} + j\frac{\pi w_1 w_2}{\lambda_0}\left(\frac{1}{r_1} - \frac{1}{r_2}\right)\right]^{-1} \tag{7}$$

For $w_1 = w_2 = w_{OUT}$, ${r_1}^{-1} = 0$ (undelayed beam) and ${r_2}^{-1} = -\Delta D/F^2$ (delayed beam) in the plane of the power detector it can be simplified to:

$$C_{inf} = \left[1 - j\frac{\pi w_{OUT}^2 \Delta D}{2\lambda_0 F^2}\right]^{-1} \tag{8}$$

The value $|C|^2$ expresses the efficiency of interfering (power coupling between the two beams), and the phase angle $\arg(C)$ gives an additional phase angle term, which denotes a kind of dispersion (the wavelength is dependent not only on frequency but additionally on path delay). Here a problem occurs: The phase angle difference of the measurement with and without the sample is firstly obtained as a path difference. Relating the path difference to the wavelength you get the phase angle difference. But the additional phase term of the overlap integral makes trouble because it is not independent from the path difference, and so only an effective wavelength can be determined. For better understanding the RF-power P_{RF}, which penetrates the cross-sectional area A_C, is concerned:

$$P_{RF} \sim \left[1 + |C_{A_C}|^2 \cos\left(\frac{2\pi}{\lambda_0}\Delta D + \arg(C_{A_C})\right)\right] \tag{9}$$

Thus an effective wavelength λ_{eff} can be defined by:

$$\frac{2\pi}{\lambda_{\text{eff}}}\Delta D = \frac{2\pi}{\lambda_0}\Delta D + \arg(C_{A_C}) \tag{10}$$

and finally the relative increase of the effective wavelength $\Delta\lambda/\lambda_0$ is given by:

$$\frac{\Delta\lambda}{\lambda_0} = \frac{\lambda_{\text{eff}} - \lambda_0}{\lambda_0} \approx -\frac{\arg(C_{A_C})\lambda_0}{2\pi\Delta D} \tag{11}$$

In fig. 3 the interference efficiency $|C_{A_C}|^2$ and in fig. 4 the relative increase of effective wavelength $\Delta\lambda_{A_C}/\lambda_0$ can be seen for the cases infinite cross-sectional area ($A_C = A_{inf}$) and cross-sectional area equal to the sensitive area of the power detector ($A_C = A_{det}$) versus path delay ΔD. The first case illustrates what would happen, if the power detector had a sensitive area with infinite dimensions. Thus it serves as a reference for comparison. The efficiency goes down to 87% for maximum path delay (which would also cause a reduction of power detector signal to 87%), the effective wavelength is slightly increased and the relative increase varies from 0.45×10^{-3} to 0.62×10^{-3}. A similar effect of a seeming increase of wavelength is known from the theory [10] of the Michelson interferometer.

For the finite cross section ($A_C = A_{det}$) apparently the interference efficiency approaches unity and on the contrary the dispersion increases. This feature rarely mentioned before has to be taken into account possibly in the phase angle evaluation, if the measurement accuracy of ε_r should be exceeded to 10^{-3} or 10^{-4}. In the following chapter of this publication another phenomenon affecting the measurement accuracy

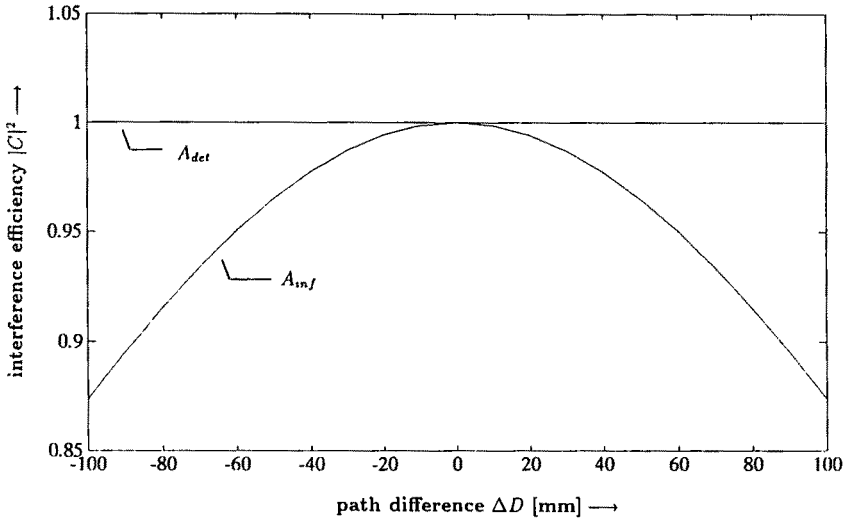

Figure 3: Interference efficiency due to the overlap integral

much more is presented. So the influence of the phase angle term of the overlap integral is neglected here. Consequently a certain amount of spill over enables a constant beam coupling of the delayed beam to the power detector and an improved interference of delayed and undelayed beam over the detector area. As conclusion in fig. 5 an interferogram is presented, which shows a constant envelope of the detector signal (dc-component removed) over a length of 200 mm.

5 Harmonic Distortion

The measurement system as mentioned in chapter 3 is an interferometer, and so a perfect sinusoidal detector signal in dependence upon path delay is expected. The special beam guiding system shown in the previous chapter allows to record this signal over 200 periods (see fig. 5). So it makes sense to evaluate the spectrum of the signal by a fast Fourier transformation with a sufficient resolution.

In fig. 6 the RF spectrum (Blackman window is applied) normalized to the fundamental and versus the wavenumber $k = 1/\lambda$ is to be seen. The axis of ordinates is scaled in RF power, as if the measurement sy-

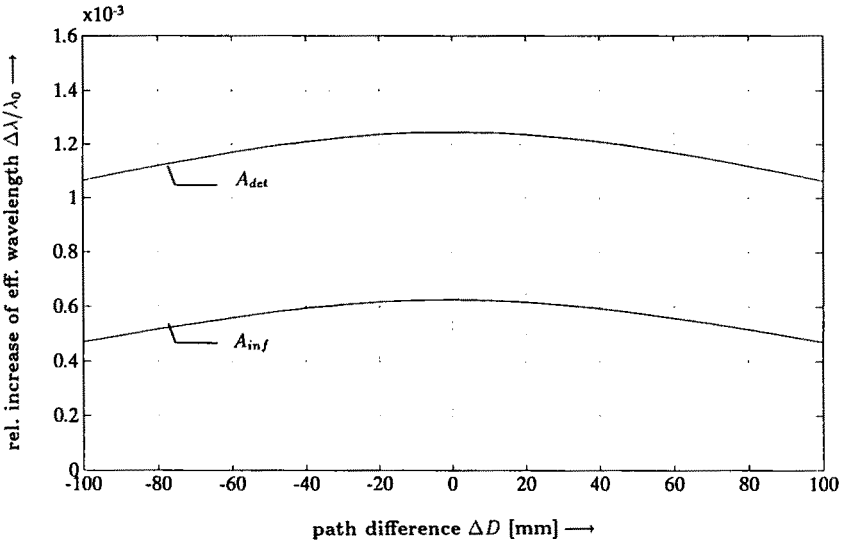

Figure 4: Increase of effective wavelength due to the overlap integral

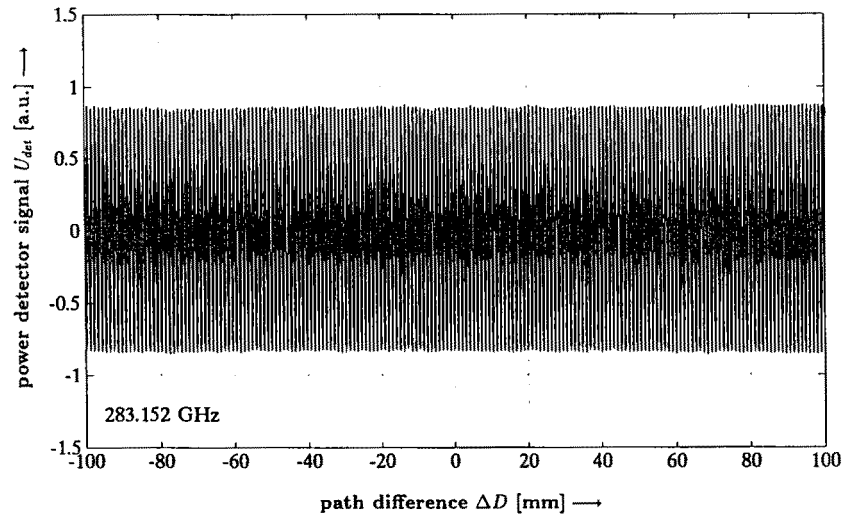

Figure 5: Interferogram over a length of 200 mm

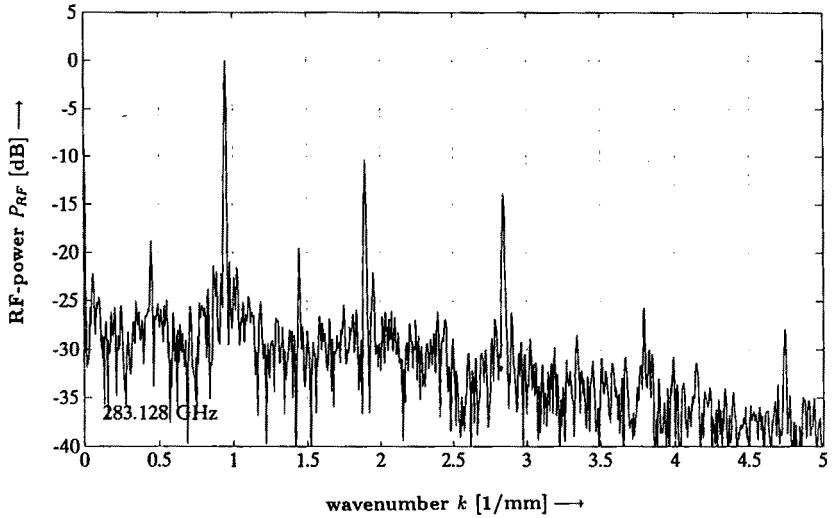

Figure 6: Spectrum of an interferogram

stem works as a spectrum analyzer ($U_{det} \sim P_{RF}$, therefore only the half dynamic range!). What you would expect is one peak at the wavenumber $k = 1/\lambda_0$ of the RF above some noise. But you get some spurious frequencies! Apparently an harmonic distortion of the single frequency signal occurs besides an amplitude or phase modulation. The amplitude or phase modulation is caused by the lead screw, which is slightly bent. But what is the reason for harmonic distortion? An hint is given in [11]. It is shown that multiple reflections between sample and Michelson interferometer produce a spectrum distortion. In our measurement system similar reasons [12] are given: imperfect source and load match. In fig. 7 an equivalent microwave circuit of the dual beam interferometer is shown. It is assumed that unused ports are perfectly matched. With given detector reflection coefficient r_D, source reflection coefficient r_S, propagation constant $\beta = 2\pi/\lambda_0$ and path delay ΔD the power P_D^{abs} (normalized to the source power P_Q), which is absorbed by the detector results in:

$$\frac{P_D^{abs}}{P_Q} = \frac{[1- \mid r_D \mid^2][1 + \cos(\beta \Delta D]}{|2 + r_S r_D \exp(-j\beta\Delta D)[1 + \cos(\beta\Delta D)]|^2} \qquad (12)$$

If a perfect source and load match $r_S = r_D = 0$ are given, the absorbed

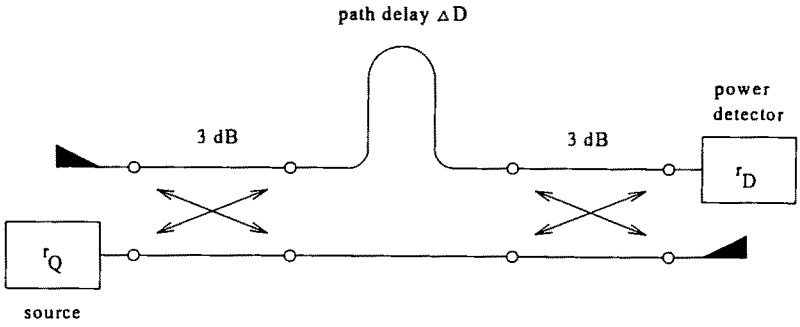

Figure 7: Equivalent microwave circuit of interferometer

power P_D^{abs} simplifies to:

$$\frac{P_D^{abs}}{P_Q} = \frac{1}{2}[1 + \cos(\beta \Delta D)] \tag{13}$$

Thus the sinusoidal behavior which is expected in general is to be seen. But in case of imperfect source and load match equ. (12) gives a distorted sinusoidal signal and the distortion is evaluated numerically. In tab. 2 the spurious harmonic power content normalized to the signal power (fundamental harmonic) is presented in dependence of various combinations of source/load match for the case phase angle $\arg(r_S r_D) = 0$.

		$10\log_{10}(P_\nu/P_1)$ in dBc			
$20\log_{10}(\sqrt{r_S r_D})$		-10	-20	-30	-40
Harmonic	2	-9.9	-20.0	-30.0	-40.0
number	3	-17.1	-26.1	-36.0	-46.0
ν	4	-24.7	-44.3	-64.3	-84.3
	5	-35.1	-52.3	-72.1	-92.0
	6	-40.1	-69.1	-99.0	-129.0
	7	-55.7	-78.5	-108.1	-138.1

Tabular 2: Harmonic content due to imperfect source/load match

Obviously the ratio of P_2/P_1 is a direct measure for $\sqrt{r_S r_D}$. Furthermore it is noticed that the harmonic power content of the spectrum

shown in fig. 6 corresponds with the conclusion of equ. (12) in the case of $20\log_{10}(\sqrt{r_S r_D}) \approx -9$ dB and a phase angle $\arg(r_S r_D) \approx 135$ degree in good agreement. By inserting an attenuation in the optical path and then inserting the same attenuation in the waveguide between carcinotron and horn antenna (that means measurement at same RF power level) it was proved that reflections between detector and horn antenna are really the reason for above mentioned phenomenon. In the latter case there is harmonic distortion, in the former case there is no. So it is shown, that the reasons are not: nonlinearity of the power detector (inclusively amplifier), periodic sampling errors [13] and also reflections in the carcinotron itself.

But what does imperfect source/load match matter? Therefore the interferometer with the sample and the reflections at horn antenna and detector are simulated by a commercial microwave design system TOUCHSTONE (the Gaussian beams are approximated by plane waves). In fig. 8 the insertion loss a and the insertion phase angle φ of the sample are shown in dependence of frequency for perfect and imperfect source/load match in the case of typical values: $\varepsilon_r = 2.12$, $\tan\delta = 2 \times 10^{-3}$, sample thickness $l_S = 5.07$ mm, distance sample to rooftop mirror $l_l = 80$ mm, distance horn antenna to detector $l_{HD} = 1000$ mm and source/load reflection of $20\log_{10}(\sqrt{r_S r_D}) = -20$ dB.

The curve with the slow variation is for the case of perfect source/load match. The slow variation is produced by the Fabry-Perot effect of the sample. The other curve with the rapid variation results from internal reflections between horn and detector which are separated by a much greater distance than the thickness of the sample, and therefore the interferences are rapid. The real electrical length between horn antenna and detector is unknown, because e.g. the unknown electrical length of a lens. Therefore if you measure at a single frequency, you don't know at which point of the curve with the rapid variation you are! Even at $20\log_{10}(\sqrt{r_S r_D}) = -20$ dB you have to tolerate a phase error $\Delta\varphi$ of ± 6 degree (this gives mainly ε_r) and an amplitude error Δa of ± 1 dB (this gives mainly $\tan\delta$). The evaluating of ε_r is not strongly affected, but the evaluating of $\tan\delta$ is strongly affected, so that $\tan\delta$ may differ up to one magnitude better or worse! In tab. 3 some other insertion loss errors Δa and phase angle errors $\Delta\varphi$ are presented for some source/load matches for this typical case.

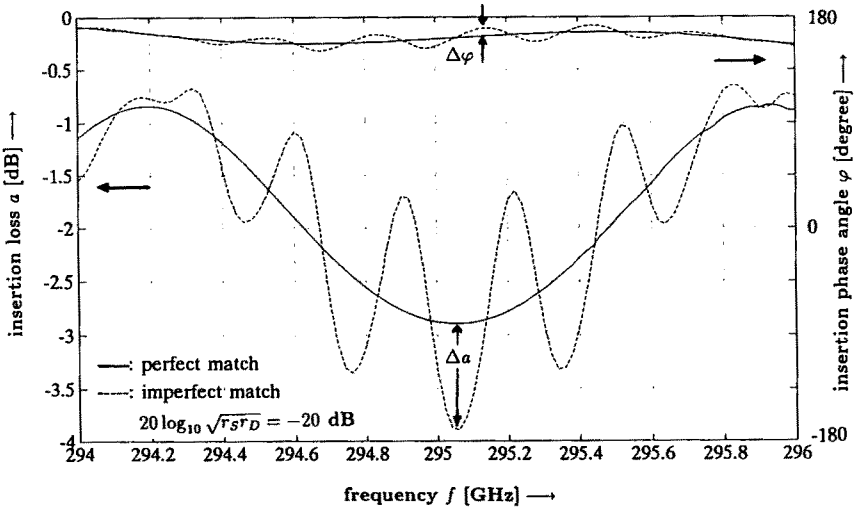

Figure 8: Insertion loss and insertion phase angle of sample

$20\log_{10}(\sqrt{r_S r_D})$	$\Delta\varphi$ in degree	Δa in dB
-20 dB	±6	±1.0
-26 dB	±3	±0.5
-30 dB	±2	±0.3
-40 dB	±0.6	±0.1

Tabular 3: Amplitude and phase angle deviations due to imperfect source/load match

This may also be a reason for great differences in published data of $\tan\delta$ of materials, to which the data of ε_r are in good agreement.

The measured value of $20\log_{10}(\sqrt{r_S r_D}) = -9$ dB in our system is unacceptable. Thus several packages of punch cards were inserted at different places in the optical path and tilted to it. The optimum was reached if every harmonic peak just vanishes in the noise floor. So a dynamic range (in network analyzer mode) of about 50 dB and a source/load match of about $20\log_{10}(\sqrt{r_S r_D}) = -25$ dB are achieved.

6 Measurements

As already mentioned in chapter 3 the measurement procedure is as follows: After a warm-up time of about one hour, and for each change of frequency of about 10 minutes, an interferogram is recorded without sample over about 50 oscillations (256 points with mirror distances of 0.1 mm). After inserting the sample the rooftop mirror starts at the same point as before, and a second interferogram is recorded with the sample. These two interferograms provide both amplitude and phase angle. Evaluation of amplitude and phase angle of the two interferogram signals is processed by a spectrum estimation routine. Such a parametric technique fits a sum of complex exponentials to the frequency domain data. It offers amplitude and phase angle of the signal with reduced statistical variance in presence of noise. The applied spectrum estimation method ([14],[15]) is a slightly modificated method of Hua and Sarkar [16]. Thus insertion loss and insertion phase angle are obtained with a high accuracy. Now these data are used to determine the dielectric constant and loss tangent. Therefore an equivalent microwave circuit of the configuration (sample, two times the distance to the fixed rooftop mirror and again sample) is simulated for plane waves in TOUCHSTONE. As modell for transmission line hollow waveguides are chosen, filled with the unknown dielectric material and air, respectively. The condition of plane waves is achieved by using hollow waveguides with a large width (in the order of 10000 λ_0). As goal for optimization the measured data of insertion loss and insertion phase angle at the frequency of measurement are taken. Then dielectric constant and loss tangent are changed by the optimization routine so that measured data correspond to simulated data. So multiple reflections and ohmic losses are taken in consideration. This is done at different frequencies and with different sample thicknesses, when available. In tab. 4 the experimental results are shown.

Material	Thickness [mm]	Frequency [GHz]	ε_r	$\tan\delta$ $\times 10^3$
Paraffin 48°C	4.87	283.388	2.264	2.0
Paraffin 48°C	4.87	294.425	2.260	8.2
Paraffin 48°C	7.92	283.387	2.260	0.6
Paraffin 48°C	7.92	294.424	2.265	2.6
Paraffin 72°C	4.63	283.389	2.272	6.0
Paraffin 72°C	4.63	294.426	2.260	10.5
Paraffin 72°C	7.41	283.388	2.268	8.2
Paraffin 72°C	7.41	294.427	2.260	7.0
TPX no. 1	5.07	283.386	2.122	1.0
TPX no. 1	5.07	294.424	2.114	1.6
TPX no. 2	5.07	283.387	2.133	2.5
TPX no. 2	5.07	294.423	2.114	0.32
Spectralon	5.45	279.723	1.724	22.5
Spectralon	5.45	292.816	1.710	22.5
Spectralon	5.45	301.539	1.728	19
Teflon	9.06	295.760	2.046	0.6
Teflon	9.06	301.548	2.038	1.1

Tabular 4: Experimental results

The main sources of errors of ε_r are errors in thickness of the samples, especially of paraffin samples, and errors in insertion phase angle φ. Due to variations of thickness in the order up to 50 μm and of insertion phase angle φ up to 3 degrees (see tab. 3) the variation of ε_r is of the order of $\Delta\varepsilon_r \approx 10^{-2}$. The main problem for determing $\tan\delta$ is the imperfect source/load match. The uncertainity of insertion loss due to a source/load match of about -25 dB is in the order of the maximum insertion loss due to the reflections of the Fabry-Perot effect and also of the insertion loss due to the actual ohmic losses of the sample. So it is clear that $\tan\delta$ varies over an order of magnitude for the samples of tab. 4 in the case of small ohmic losses.

7 Conclusion

In this paper it is shown that it is possible to determine the dielectric constant of a dielectric material with a sufficient accuracy for usual applications having a basic equipment of a (sub)mm-wave laboratory. A seldom before mentioned subject, namely imperfect source/load match

(in this system the unmatch of the corrugated horn antenna and the pyroelectric detector, respectively), is investigated thoroughly by utilizing a special beam-guiding system. A measurement method and an improvement of source/load match are proposed. Nevertheless the remaining small imperfect source/load match causes a great systematic error in data of $\tan\delta$. This may also be the reason for great variations in up to now published data of $\tan\delta$. The special beam-guiding system allows a more accurate evaluation of phase angle and amplitude with one measurement by means of a spectrum estimation method. The processing of dielectric constant and loss tangent from insertion loss and insertion phase angle is considerably simplified by using a commercial available microwave design system. At last data of some plastics are given, especially of paraffin waxes with different melting temperatures and of SPECTRALON, a kind of microcellular teflon.

8 Acknowledgement

The author would like to thank H. Brand, M. Raum for helpful discussions and suggestions, U. Martin for providing the spectrum estimation method, R. Schneider for the explanation of harmonic distortion in his diploma thesis and G. Bauer, L. Höpfel and J. Popp for careful manufacturing the measurement system.

9 Literature

[1] Simonis, G.J.: Index to the Literature Dealing with the Near-Millimeter Wave Properties of Materials; Intern. Journal of Infrared and Millimeter Waves, Vol. 3, No. 4, 1982, pp. 439 - 469.

[2] Afsar, M.N.: Dielectric Measurements of Millimeter-Wave Materials; IEEE Trans. on Microwave Theory and Techniques, Vol. MTT-32, No. 12, December 1984, pp. 1598 - 1609.

[3] Jones, C.R.; Dutta, J.M.; Davé, H.: Complex Dielectric Constants for Selected Near-Millimeter-Waves Materials at 245 GHz; IEEE Trans. on Microwave Theory and Techniques, Vol. MTT-34, No. 9, September 1986, pp. 932 - 936.

[4] Jones, C.R.; Dutta, J.M.; Davé, H.: Two-Beam Interferometer for Optical Constants Measurements at Near-Millimeter Wavelengths; Intern. Journal of Infrared and Millimeter Waves, Vol. 5, No. 3, 1984, pp. 279 - 299.

[5] Qiu Bingsheng, Liu Chengjia, Huang Jiangjun, Qiu Ruman: Automatic Measurement for Dielectric Properties of Solid Material at 890 GHz; Intern. Journal of Infrared and Millimeter Waves, Vol. 13, No. 6, 1992, pp. 923 - 931.

[6] Martin, D.H.; Puplett, E.: Polarized interferometric spectrometry for the millimetre and submillimetre spectrum; Infrared Physics, Vol. 10, 1969, pp. 105 -109.

[7] Goldsmith, P.F.: Quasioptical Techniques offer Advantages at Millimeter Frequencies; MSN, December 1983, pp. 65-84.

[8] Stöckel, B.: Derivation of Invariant Quasi-Optical Systems and Their Applications - Especially at a mm-Wave-Fourier-Transform Spectrometer; Vol. AEÜ-44, No.4, 1990, pp. 306-312.

[9] Kogelnik, H.: Coupling and Conversion Coefficients for Optical Modes; Proceedings of the Symposium on Quasi-Optics, New York, June 8-10, 1964, pp. 333 - 347.

[10] Chantry, G.W.: Submillimetre Spectroscopy; Academic Press, London and New York, 1971.

[11] Jongbloets, H.W.; Van de Steeg, M ; Van der Werf, E.J.; Stoelinga, J.H. and Wyder, P.: Spectrum distortion in far-infrared Fourier spectrometry by multiple reflections between sample and Michelson interferometer; Vol. 20, Infrared Physics, 1980, pp. 185-192.

[12] Chamberlain, J.: The principles of interferometric spectroscopy; Wiley, Chichester, 1979.

[13] Schneider, R.: Aufbau eines Autokorrelators zur Verwendung als Spektral-Analysator bei Submillimeter-Wellen; Diploma-Thesis, No. 526, 1989, Lehrstuhl für Hochfrequenztechnik, Universität Erlangen-Nürnberg.

[14] Höß H.: Parametrische Schätzung von Frequenzen und Amplituden von Mehrtonsignalen; Diploma Thesis No. XE-417, 1992, Lehrstuhl für Nachrichtentechnik, Universität Erlangen-Nürnberg.

[15] Martin, U.: Private Communications; Lehrstuhl für Nachrichtentechnik, Universität Erlangen-Nürnberg, 1992.

[16] Hua, Y.; Sarkar, T.K.: Matrix pencil method for estimating parameters of exponentially damped/undamped sinusoids in noise; IEEE Trans. Acoust., Speech Signal Process., May 1990.